Solar Energy 306 (2026) 114288

Contents lists available at ScienceDirect

Solar Energy

journal homepage: www.elsevier.com/locate/solener

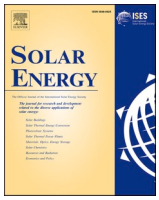

Hybrid solar collectors based on Bragg-mirror spectral splitting for simultaneous heat and electricity generation☆

Botho Lehmann, Gan Huang *

Institute of Microstructure Technology, Karlsruhe Institute of Technology, Hermann-von-Helmholtz-Platz 1, 76344 Eggenstein-Leopoldshafen, Germany

ARTICLE INFO

Keywords:
Solar energy
Spectral splitting
PV/T

ABSTRACT

Spectral-splitting photovoltaic-thermal (PVT) solar collectors offer a pathway for simultaneous electricity and high-temperature heat generation from solar energy. In this study, we experimentally investigate a PVT solar collector incorporating a dielectric Bragg mirror as a spectral-splitting optical reflector. The solar collector spectrally separates the solar spectrum by reflecting part of the spectrum (< 870 nm) to a concentrated gallium arsenide (GaAs) photovoltaic cell and transmitting the rest of the spectrum (> 870 nm) to a solar thermal absorber. The resulting spectrum splitting achieves a reflectance of 91.4 % above the GaAs bandgap and a transmittance of 79.7 % below it. Under concentrated illumination (geometric factor of 100) and based on the total incident solar energy (full-spectrum performance), the GaAs cell has an electrical efficiency of 6.5 % operating at 36.6 °C, while the solar thermal absorber achieves a thermal capture efficiency of 8.8 % at 80 °C. The stagnation temperature of the solar thermal absorber, measured experimentally without heat extraction, reaches 209.1 °C. Both electrical and thermal efficiencies remain limited, primarily due to optical losses arising from misalignment and interference-related reflection losses. The Bragg mirror exhibits negligible absorption and self-heating, confirming its suitability for spectral splitting under concentrated illumination. While such optical losses remain challenges for both the indoor prototype and potential outdoor implementations, this work highlights a strategy for enhancing hybrid solar energy utilisation.

1. Introduction

Meeting global climate targets demands a rapid transition away from fossil fuels in both the electricity and heat sectors, which together account for the majority of final energy consumption. In particular, thermal applications such as space heating, water heating, and industrial processes represent nearly 50 % of final energy demand, surpassing both electricity and transportation sectors [1]. Despite the growing share of renewables, heat and power production remain major sources of greenhouse gas emissions. This underscores the need for innovative solar technologies capable of addressing both electricity and heat demands efficiently [2].

Photovoltaic-thermal (PVT) technologies represent a compelling solution by enabling the co-generation of electricity and useful thermal energy from a single solar collector. In conventional PVT collectors, the photovoltaic (PV) module is thermally coupled to a heat absorber that recovers waste heat while simultaneously cooling the PV cell, improving electrical performance. This configuration can achieve combined system efficiencies above 80 % [3]. According to a study by Fraunhofer ISE, compared with a side-by-side installation of separate PV (~70 %) and solar thermal (~30 %) collectors, a PVT collector can deliver the same amount of heat while generating more than twice as much electricity [4]. While at room temperature, a single junction silicon photovoltaic (PV) cell under one sun has the world-record efficiency of 27.8 % by LONGi [5], with the rest of the incident energy (>60 %) dissipated as waste heat. The champion silicon PV module from LONGi exhibits an efficiency of 26.0 % [6], which is about 1.8 % lower than that of the record cell due to reflection, packing ratio, and resistive losses. Concentrated photovoltaic (CPV) systems can reach even higher efficiencies of above 40 % (under direct light); however, they face several challenges, including higher capital costs, significant thermal loads, and the inability to utilize diffuse solar radiation. However, the coupling of the PV cell and thermal absorber in conventional PVT collectors imposes a constraint: increasing the thermal output temperature typically elevates the PV cell temperature, reducing its efficiency. As a result, most commercial PVT systems operate below ~85 °C and are restricted to

☆ This article is part of a special issue entitled: 'Solar-to-X' published in Solar Energy.

* Corresponding author.
E-mail address: gan.huang@kit.edu (G. Huang).

https://doi.org/10.1016/j.solener.2025.114288
Received 26 September 2025; Received in revised form 14 December 2025; Accepted 22 December 2025
Available online 31 December 2025

low-temperature applications such as domestic water or space heating [7,8].

To overcome this trade-off, spectral-splitting PVT solar technologies have emerged as a promising alternative [9]. These systems optically separate the solar spectrum, directing high-energy photons (UV–visible) to the PV cell and transmitting lower-energy photons (near- and mid-IR) to the thermal absorber. This decouples the thermal and electrical receivers, allowing the thermal subsystem to reach higher temperatures while minimising the thermal load on the PV cell. However, spectral-splitting introduces additional optical losses and complexity in system integration, especially under concentrated sunlight [9], which requires precise solar tracking and depends solely on direct normal irradiance (DNI) for effective focusing. Nevertheless, the potential for simultaneous high-temperature heat and efficient electricity generation makes spectral-splitting PVT collectors an attractive approach for deep decarbonisation [10]. Additionally, the concentrated irradiance elevates the open–circuit voltage of the PV cell, thereby enhancing electrical efficiency [10–12]. Recent advances in spectral-splitting PVT technologies have been summarised in several review articles [13–17].

Two main classes of optical filters are employed in spectral-splitting systems. The first includes selectively absorptive liquid-based filters, often using nanofluids with tailored absorption spectra [18–21]. Nanoparticles (e.g., ZnO [22,23], Ag [24], polypyrrole [25], CNTs [26], ZnO/SiO_2 [27], carbon quantum dots [28]) suspended in a base fluid absorb UV or IR radiation and transfer the absorbed heat directly to the fluid [14,29]. Extensive and significant efforts have been made to enhance spectral selectivity and thermal transfer in such filters [30–36]. More research on nanofluid-based spectral splitting PVT collectors can be found in recent review papers [37]. The second and more mature class consists of dielectric multilayer filters or Bragg mirrors, which rely on interference effects from alternating layers of high and low refractive index materials (e.g., TiO_2 and SiO_2) to reflect desired wavelengths and transmit others [38–41]. These mirrors exhibit minimal self-heating, are widely tuneable via design, and are compatible with scalable fabrication techniques such as inkjet printing [42,43]. The spectral-splitting PVT collectors based on Bragg mirrors are also integrated with thermoelectric generator (TEG) [44,45], thermophotovoltaics [46], and plant growth [47]. The Bragg mirror can be positioned near the focal point [21,48] or directly integrated onto the curved surface of the PV cell, serving simultaneously as an optical filter and a solar concentrator [49]. In recent years, the use of semi-transparent photovoltaic cells as optical filters has also emerged as a promising approach for spectral splitting [50–53].

A challenge in deploying Bragg mirrors under solar concentration is their strong angular dependence. The effective optical thickness of the mirror varies with the angle of incidence, causing a blue shift in the reflection band. In concentrated systems, where the incident light spans a wide angular range due to the focusing optics, this angular shift can distort the spectral separation and reduce overall efficiency [55]. However, the impact of angular mismatch between the conical or pyramidal solar concentrated beam and the Bragg mirror in spectral-splitting PVT collectors has not been comprehensively investigated, despite its importance for realistic system integration and performance optimisation.

In this study, we experimentally demonstrate a spectral-splitting PVT collector integrating a Bragg mirror as a spectral-splitting optical reflector. The collector is designed to reflect ultraviolet and visible light (<870 nm) to a GaAs PV cell and transmit infrared light (>870 nm) to a solar thermal absorber thermally coupled to a copper storage block. We conduct detailed angular-resolved optical characterisation of the Bragg mirror and perform ray-tracing simulations to evaluate incident angle distributions under concentration. The prototype collector is tested under a solar simulator (class AAA, *Wacom*) to assess electrical and thermal performance, highlighting the role of optical alignment, spectral filtering, and thermal design in achieving efficient solar co-generation.

2. Experimental methodology

2.1. The design of spectral splitting PVT collector employing a Bragg mirror

The concept of spectral-splitting PVT using a dielectric Bragg mirror is demonstrated in this study. As illustrated in Fig. 1a, the sunlight is concentrated by a Fresnel lens and directed onto the Bragg mirror. The Fresnel lens is made of polymethylmethacrylate (PMMA), with a square aperture of 100 × 100 mm^2 and a focal length of 90 mm. The Bragg mirror transmits the infrared (IR) portion of the solar spectrum to a solar thermal absorber that is thermally coupled to a copper storage block. These components are housed within a vacuum chamber to minimise thermal losses. Simultaneously, the remaining spectrum, primarily ultraviolet (UV) and visible light, is reflected to a GaAs cell for electricity generation. Due to the high optical concentration (geometric factor of 100), the GaAs cell is actively cooled using nitrogen gas. The Bragg mirror functions as a beam splitter with the cutoff wavelength λ_b, meaning wavelengths shorter than λ_b are reflected to the GaAs cell while longer wavelengths are transmitted to the solar thermal absorber, as shown in Fig. 1b.

The structure of the solar thermal absorber vacuum chamber is made from polymethylmethacrylate as presented in Fig. 1c. The light enters the chamber through a 0.5-mm-thick fused silica glazing and reaches the 0.2-mm-thick solar thermal absorber material (*Alanod EtaPlus*), which is soldered to a thermal storage block made from copper (lead-free solder: *Felder ISO-Core "Clear" Sn100Ni*$^+$). The copper block is suspended via a frame made of silica to minimise conductive losses, and its temperature is monitored via a thermocouple. Additionally, the inner walls of the chamber are covered with low-emissivity mirrors and the polymethylmethacrylate housing is insulated with extruded polystyrene covered with aluminium tape, shown in Supplementary Fig. 1. This insulation method hinders all three forms of heat transfer. The prototype presented in this study is a small-scale system tested under a solar simulator. The solar thermal absorber has an area of only 14 × 14 mm^2, absorbing a relatively small amount of energy. Under such conditions, implementing a flowing heat extraction system is challenging, as the required mass flow rate would be extremely low and difficult to control or measure accurately. Therefore, a thermal storage block was used to store the absorbed heat, and the thermal capture efficiency was determined from the measured temperature gradient. In future large-scale studies, a dedicated heat exchanger will be integrated with the solar thermal absorber to enable continuous heat extraction and more realistic system evaluation.

The GaAs cell is encapsulated in a polydimethylsiloxane-sealed housing with a 0.5-mm-thick silica glazing and mounted on a 0.5-mm-thick copper substrate for better heat dissipation. The silica cover is required to hermetically encapsulate the GaAs PV cell and protect it from ambient air exposure, preventing surface oxidation and performance degradation during operation. Nitrogen gas flows at 25 L/min across the rear of the copper substrate to maintain safe operating temperatures under concentrated irradiance. The copper plate is coated with black paint to increase the thermal emissivity for the infrared temperature sensor, which is calibrated before the experiment. The complete encapsulation is shown in Fig. 1d and is more detailed in Supplementary Fig. 2.

In this study, the Fresnel lens made of PMMA is employed solely for prototype fabrication and indoor testing under controlled laboratory conditions. For future outdoor testing and practical applications, more durable concentrator materials will be adopted to ensure long-term optical and mechanical stability under ultraviolet exposure. Suitable alternatives include Fresnel lenses made of UV-stabilized glass or commercially available parabolic solar concentrators, which offer superior resistance to UV-induced degradation and maintain high performance over extended operational lifetimes. In this prototype, N_2 gas cooling is employed solely to maintain a stable temperature of the

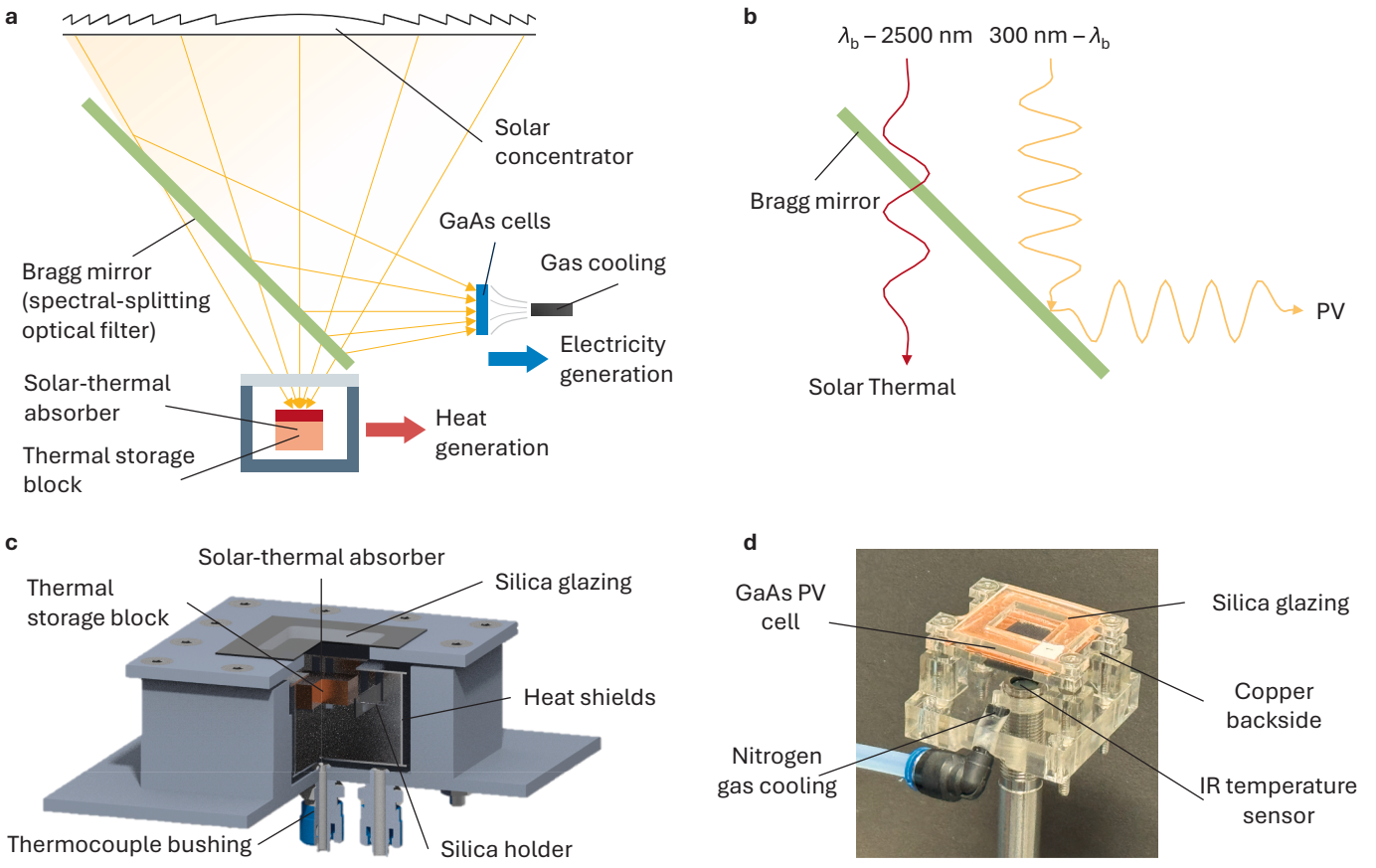

Fig. 1. Design and implementation of the spectral–splitting PVT collector using a Bragg mirror. a, Schematic of the spectral–splitting PVT system. A Fresnel lens concentrates sunlight onto a dielectric Bragg mirror. A part of the spectrum is transmitted to a solar thermal absorber for heat generation, while the rest of the spectrum is reflected to a gas-cooled, concentrated GaAs PV cell for electricity generation. **b**, Details of the Bragg mirror spectral splitting. A dielectric stack engineered for cutoff wavelength λ_b, ideally matched to the PV bandgap, reflects $\lambda < \lambda_b$ toward the PV cell and transmits $\lambda > \lambda_b$ to the thermal absorber. **c**, Cross-section of the solar thermal absorber housing. A polymethylmethacrylate vacuum enclosure capped with a fused silica glazing. Mirrored inner walls to reduce thermal radiation loss. Two 0.5-mm-thick silica frames are used to support the solar thermal absorber to minimise conductive and radiative losses. An embedded thermocouple is used for temperature monitoring. **d**, Photograph of the fabricated GaAs PV module with active gas–cooling and an infrared temperature sensor for temperature measurement.

concentrated GaAs PV cell, without recovering the associated waste heat. In future large-scale implementations, liquid coolants such as water or heat transfer oil could be used instead, enabling efficient heat recovery from the PV module [54]. Integrating a high-efficiency heat exchanger would allow this recovered heat to be utilized for domestic or industrial applications, thereby improving the overall system efficiency.

2.2. Optical, electrical and thermal characterisation methods

2.2.1. Optical characterisation

Comprehensive characterisation of the optical components was performed using a UV–Vis–NIR spectrophotometer (*Agilent Cary 7000*). The instrument is equipped with a dual-lamp light source, comprising a quartz tungsten halogen lamp for the visible and near-infrared (NIR) regions and a deuterium arc lamp for the ultraviolet (UV) range, to ensure accurate spectral coverage from 250 nm to 2500 nm. An integrating sphere is used to collect both diffuse and specular components of reflectance and transmittance. To resolve angular dependencies of the dielectric Bragg mirror, a universal measurement module is employed, capable of quantifying direct transmission and reflection at incident angles ranging from 15° to 80°. The spectral data acquisition interval is maintained at 10 nm, consistent with the standard spectral measurements performed in the integrating sphere mode. For spectral weighting and performance prediction, measured reflectance and transmittance spectra are pointwise multiplied by the standard AM1.5D solar spectrum, enabling quantification of spectrally resolved absorption and optical power delivered to the PV and thermal receivers under concentrated sunlight conditions.

2.2.2. Electrical characterisation

The electrical performance of the GaAs PV cell under concentrated solar illumination is characterized using a continuous dual-lamp solar simulator (class AAA, *Wacom*) comprising a xenon arc lamp (*Wacom KXL-500F*) and a halogen lamp (*Ushio JC-36 V-400 W*). The spectral output is calibrated to closely match the AM1.5G reference spectrum and the irradiance is adjusted to 1000 W/m^2 (calibrated by a pyranometer) over the 100 × 100 mm^2 illuminated area. Electrical measurements are conducted using a high-precision source meter (*Keithley 2618B*) capable of sourcing and measuring voltage and current with high temporal resolution. Given the high optical flux and dynamic thermal behaviour of the GaAs cell, initial I-V measurements are performed every 15 s, sweeping the voltage from 0.4 V to the open-circuit voltage (V_{OC}) in 0.05 V increments over 50 cycles to capture transient response. Thereafter, steady-state measurements are conducted at 5-minute intervals using a finer voltage step size of 0.01 V across the entire operational range. This dual-scale approach ensures accurate characterisation of both dynamic and stabilised electrical output.

2.2.3. Thermal characterisation

Thermal performance is assessed by simultaneous temperature

monitoring of both the copper thermal storage block and the encapsulated GaAs PV cell. Type T thermocouples are attached to the thermal storage block and interfaced with a TC-08 data logger (Pico Technology) sampling at 1 Hz. For non-contact temperature monitoring of the PV cell encapsulation, an infrared (IR) sensor (*Optris GEN CSS LE*) is positioned to record the rear surface temperature. To ensure high emissivity and minimise IR measurement error, the rear surface of the encapsulation is coated with black spray paint. Sensor calibration is carried out by concurrently recording temperatures with a thermocouple embedded near the cell and the IR sensor during controlled heating, yielding an agreement within ±1 K. To further quantify the thermal gradient between the measured encapsulation surface and the actual PV junction temperature, a control experiment is conducted using an identical encapsulation geometry with an embedded thermocouple in the absorber (Alanod EtaPlus). The resulting offset is documented in Supplementary Fig. 6 and confirms that the GaAs cell remained within safe operating limits during testing. All temperature data are recorded continuously at 1 Hz until thermal steady state is reached, defined as a temperature gradient below 1 K per hour. Concurrent thermal and electrical characterisations are conducted under identical illumination conditions using the solar simulator. The thermal capture efficiency is computed from the rate of temperature increase in the thermal storage block, based on its measured thermal mass (10.5 g) and the specific heat capacity of copper (385 J/kg·K). The temperature gradient is averaged over 25-second intervals to reduce experimental noise. Variations in heat capacity due to temperature or minor contributions from coatings and solder are neglected. A uniform temperature distribution within the copper block is assumed, justified by its high thermal conductivity. All efficiency values are normalised to the total direct energy input of 10 W from the solar simulator. The initial thermal transients are excluded to focus exclusively on quasi-steady-state behaviour.

3. Results and discussion

3.1. Optical properties of the Bragg mirror in the spectral-splitting PVT solar collector

The Bragg mirror appears visibly reflective due to its high reflectance in the UV–visible spectrum (Fig. 2a). The GaAs cell is clearly visible in reflection, while the thermal absorber is hidden from view behind the mirror. Because the mirror is illuminated by a Fresnel lens, the incident light spans a broad angular range. Therefore, the angular-dependent, spectrally weighted transmittance and reflectance of the Bragg mirror are characterised in this study. Fig. 2b shows transmittance curves from 15° to 80° incidence. Below 870 nm, transmittance remains low (<0.2 % at 15°), while above 870 nm it rises to 78.1 % at 15°, peaks at 82.6 % at 60°, then declines to 23.5 % at 80°. This behaviour shows a blue shift in the cutoff wavelength and the increasing reflectance with increasing angle. The corresponding reflectance in the 300 to 870 nm range, shown in Fig. 2c, decreases slightly from 95.4 % to 88.3 % across the same angular range.

To quantify the actual angle distribution at the Bragg mirror's surface, a ray-tracing simulation in MATLAB for a Fresnel lens with a 90 mm focal length and a size of 100 × 100 mm^2 is conducted. A total of 0.25 million rays are generated uniformly across the lens surface, and their angles upon intersecting the 45°-tilted mirror plane are computed. In the representation in Fig. 2d, the light beams and the Bragg mirror are shown for demonstration purposes for 25 light beams. The resulting angle distribution for 0.25 million rays, shown in Fig. 2e, ranges from 15.9° to 75.7°, with an average of 47.7°, slightly higher than the geometric 45° due to Fresnel lens curvature.

To calculate the final average properties of the Bragg mirror, the results from Fig. 2b and Fig. 2c are interpolated linearly to achieve a transmittance and reflectance for every angle between 15° and 80° as well as all wavelengths between 300 nm and 2500 nm. The 3-

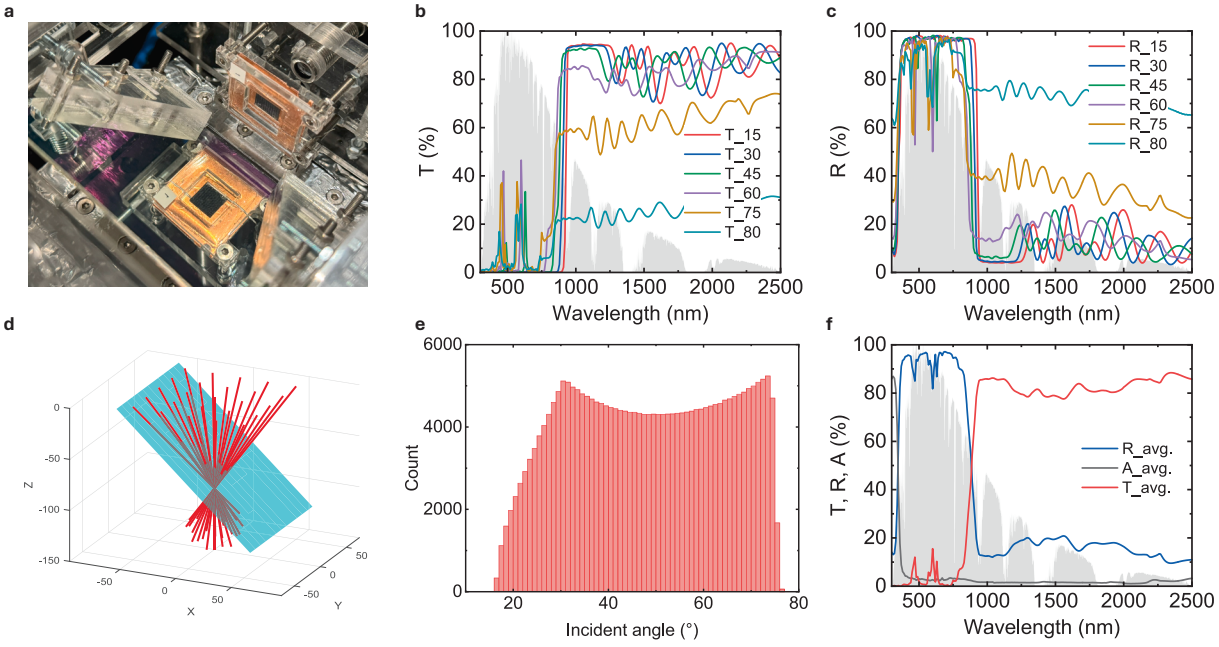

Fig. 2. Optical characterisation of the Bragg mirror. a, Photograph of the Bragg mirror under broadband illumination, appearing as a mirror for visible light since its cutoff wavelength $\lambda_b > 780$ nm. **b**, Transmittance spectra of the Bragg mirror measured at 15°–80°, showing overall transmittance decline and a spectral blueshift of the cutoff λ_b toward shorter wavelengths with increasing incident angle. **c**, Reflectance spectra of the Bragg mirror measured at 15°–80°, illustrating high reflectance at $\lambda < \lambda_b$ and increasing further as the angle deviates from normal incidence for $\lambda > \lambda_b$. **d**, Ray–tracing simulation of the pyramidal-shaped concentrated light beam on an inclined Bragg mirror. 3-dimensional view of 25 rays focused by a Fresnel lens onto the Bragg mirror tilted at 45° to the central beam, demonstrating a range of incident angles across the reflector surface. **e**, The incident angle distribution for 0.25 million simulated rays, revealing that most rays strike the reflector at angles substantially different from 45°. **f**, Average transmittance and reflectance spectra of the 45°-tilted Bragg mirror for the pyramidal-shaped concentrated sunlight (weighted results based on the distribution in Fig. 2e).

dimensional plot of transmittance, reflectance and absorption over the angles and wavelengths is shown in Supplementary Fig. 3. The results are summarised in Fig. 2f, showing a weighted transmittance of 79.7 % above 870 nm and a weighted reflectance of 91.4 % below it. Optical losses, primarily from absorption and scattering, account for 2.5 % across 375–2500 nm, increasing to 40.4 % for 300–375 nm (3.2 % overall). The effective cutoff wavelength is 870 nm, well-matched to the GaAs bandgap.

3.2. Optical characterisation of the Fresnel lens and solar thermal absorber

The Fresnel lens transmits 88.5 % across the 300–2500 nm range, consistent with polymethylmethacrylate optical properties as shown in Fig. 3a. The optical losses created by the micro-grooved design of the Fresnel lens are not measured in this study.

The solar thermal absorber exhibits a broadband absorption of 94.9 % under the full solar spectrum (Fig. 3b). To achieve higher-temperature heat generation, the solar thermal absorber is placed inside a thermally insulated vacuum chamber sealed with a fused silica window. The fused silica glazing is positioned around 5 mm above the absorber surface and does not contact the absorber directly. This configuration aims to suppress convective heat losses and reduce radiative losses, which is particularly important given the small solar-thermal absorber area and the limited optical concentration provided by the Fresnel lens. Fused silica is selected for its high transmittance across the solar wavelength range and its sufficient mechanical strength to maintain a stable vacuum environment. The transmittance and reflectance spectra of the fused silica window remain nearly constant across the solar wavelength range of 300–2500 nm, ensuring minimal influence on the spectral-splitting process. The measured optical spectra of the silica glazing are provided in Supplementary Fig. 4. Fig. 3c shows the combination of all measured optical effects, as we compute the effective spectral distribution incident on each component under AM1.5D conditions (representing direct normal sunlight at an air mass of 1.5), where only the direct component is considered because it is the portion of the solar spectrum that can be concentrated. Using the data from Fig. 3c, the overall energy flow and distribution within the system have been quantified and are illustrated in Fig. 3d. The GaAs cell receives 5.3 W over a 10×10 mm^2 area, while the solar thermal absorber receives 2.1 W over 14×14 mm^2. Total system losses from optical elements are estimated at 1.5 W, consisting of losses in the Fresnel lens, Bragg mirror and the fused silica encapsulation as well as the fused silica window of the solar thermal absorber housing.

3.3. Performance of the spectral-splitting PVT collector with a concentrated GaAs cell

The experimental setup without the Fresnel lens is shown in Fig. 4a, and the simulated optical paths are visualised in Fig. 4b using *COMSOL Multiphysics* ray tracing. With an ideal focus point of the Fresnel lens, the GaAs cell can be placed further away from the focus point to increase the distance between the components, allowing better alignment and thermal decoupling. Due to real-world deviations from ideal lens focusing, component alignment is performed manually under solar simulator illumination to ensure correct spectral splitting and optical power

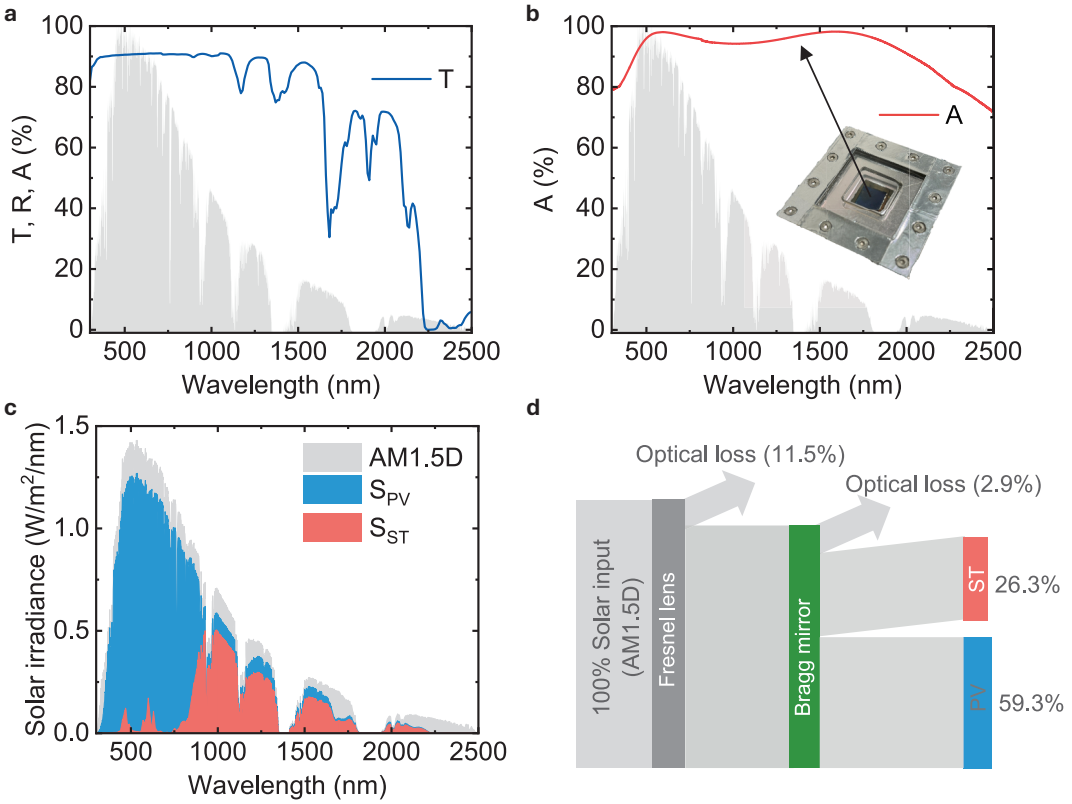

Fig. 3. Optical characterisation of the Fresnel lens and solar thermal absorber. a, Transmission spectrum of the polymethylmethacrylate Fresnel lens, isolating material-induced losses across the solar spectrum independent of groove geometry. **b**, Absorption spectrum of the solar thermal absorber, demonstrating near–unity absorption throughout the operational band with minor edge–region roll–off. **c**, Resulting spectral–splitting under the AM1.5D standard spectrum. It shows the transmitted wavelengths ($\lambda > \lambda_b$) directed to the PV cell (S_{PV}), transmitted wavelengths ($\lambda < \lambda_b$) harvested thermally (S_{ST}), and quantified optical losses. **d**, Energy flow and distribution in the hybrid Bragg-mirror spectral-splitting system. Around 11.5 % of the incident AM1.5D irradiance is lost due to reflection and absorption in the Fresnel lens. The Bragg mirror reflects and transmits the majority of the remaining light, while only 2.9 % of the incident AM1.5D irradiance is absorbed by the Bragg mirror itself. After spectral splitting, around 26.3 % of the incident energy reaches the solar-thermal collector (with the silica glazing), and 59.3 % reaches the PV collector (with the silica glazing).

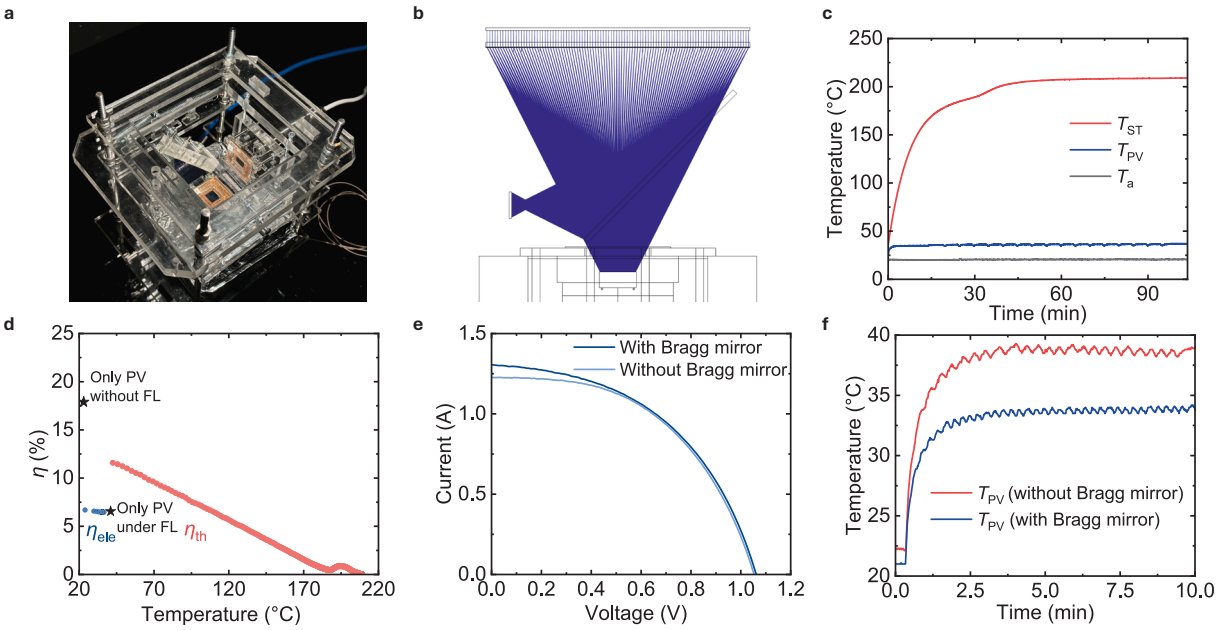

Fig. 4. Electrical and thermal performance of the spectral–splitting PVT collector. a, Photograph of the experimental setup, showing the Bragg mirror, and gas-cooled GaAs PV cell (the solar thermal absorber lies behind the reflector, and the Fresnel lens is removed for better visibility of the internal structure). **b**, Ray–tracing simulation illustrating ideal light pathways to the GaAs cell and the solar thermal absorber. **c**, Temperature curve of the solar thermal (T_{ST}) and the GaAs cell (T_{PV}) during operation. **d**, Electrical and thermal efficiencies of the spectral–splitting PVT collector versus a PV–only baseline (thermal capture efficiency curve is smoothed over 25 s to reduce noise), with electrical efficiency plotted as a function of PV cell encapsulation temperature and thermal capture efficiency plotted as a function of solar thermal temperature. The "only PV without FL" refers to the PV baseline tested without solar concentration, while the "only PV with FL" refers to the PV cell tested under concentrated illumination using the Fresnel lens, with active nitrogen gas cooling. **e**, Current–voltage (I–V) characteristics of the GaAs cell with and without the Bragg mirror. It shows a negligible performance change of the electrical efficiency between these two configurations. The "with Bragg mirror" configuration corresponds to the system under the Fresnel lens with spectral splitting, whereas the "without Bragg mirror" configuration corresponds to the same system under the Fresnel lens but without the Bragg mirror. **f**, GaAs cell encapsulation temperature profile with active gas cooling, demonstrating the Bragg mirror's role in lowering cell operating temperature.

distribution.

Temperature profiles of the solar thermal absorber (the copper block), GaAs cell, and ambient are plotted in Fig. 4c. The thermal block reached a peak temperature of 209.1 °C. The gradient change at ~190 °C can be attributed to solder melting at the absorber-block interface. The GaAs cell remained below 37.0 °C throughout the experiment, with minor fluctuations caused by current–voltage (I–V) measurements every 5 min.

Thermal capture efficiency is calculated using the temperature gradient and the heat capacity of the copper block (neglecting minor contributions from coating and solder). The heat capacity is assumed to be constant over the temperature range, and the temperature changes throughout the copper block are assumed to be the same because of the copper's high heat transfer coefficient. Results in Fig. 4d indicate thermal efficiencies of 11.7 % at 40 °C, 8.8 % at 80 °C, and 3.2 % at 150 °C. The efficiency spike at 190 °C, corresponding to solder melting, is excluded from performance evaluation.

The GaAs cell achieved an electrical efficiency of 6.7 % at 23.9 °C, declining slightly to 6.5 % at steady-state operation (36.6 °C). The bare non-concentrated GaAs PV cell achieves an electrical efficiency of 17.9 % at an operating temperature of 22.0 °C, under identical nitrogen gas cooling. However, with solar concentration via the Fresnel lens, the efficiency drops significantly to 6.5 % at 41.0 °C. This 63.7 % reduction is attributed to three primary factors: (i) optical losses, including 8.4 rel. % from the Fresnel lens material and 7.1 rel.% from the fused silica cover due to non-directly transmitted light; (ii) a 47.4 rel.% efficiency loss resulting from elevated cell temperature, based on the temperature coefficient of GaAs PV cells [56–58]; and (iii) optical misalignment and geometric losses – specifically, suboptimal positioning of the GaAs PV cell relative to the Fresnel focus, as well as intrinsic design limitations of the Fresnel lens grooves, which lead to internal optical losses independent of the material itself (37.1 rel.%). Given the 1 cm^2 active area, even minor misalignments significantly impact performance, as discussed in Supplementary Fig. 5, and the estimation of the temperature difference between the encapsulation and the GaAs cell is shown in Supplementary Fig. 6.

The experimental I–V curves in Fig. 4e show consistent electrical output between the configurations with and without the Bragg mirror, indicating that spectral filtering losses (~8.6 % below 870 nm) are compensated by the reduced cell temperature from 39.4 °C to 34.2 °C, as seen in Fig. 4f. The fluctuations in the GaAs cell temperature graphs are due to the changing load when measuring the I–V curves in a measuring interval of 15 s. The relatively low fill factor observed in Fig. 4e is primarily attributed to overheating of the GaAs cell under concentrated illumination, which causes a reduction in open-circuit voltage. Although the measured temperature on the back of the encapsulated PV module was only 37 °C, the actual temperature of the GaAs material is expected to be considerably higher, as shown in Supplementary Fig. 6. In addition, high optical concentration can increase resistive losses within the cell contacts and semiconductor layers, further lowering the fill factor. The performance of the same GaAs cell under non-concentrated (one-sun) conditions, presented in Supplementary Fig. 5, confirms that its intrinsic fill factor is significantly higher. These results indicate that the reduced fill factor in the current experiment arises mainly from thermal effects and concentration-induced resistive losses rather than from the inherent properties of the cell.

We summarize and compare reported experimental studies on Bragg-mirror-based spectral-splitting PVT systems in Table 1. The comparison includes the type of solar concentrator, electrical efficiency, thermal efficiency at a given operating temperature, and maximum heat temperature achieved. Although theoretical studies suggest that Bragg-mirror-based spectral-splitting PVT systems can potentially achieve

Table 1
Summary of electrical and thermal efficiencies of Bragg-mirror-based spectral-splitting PVT collectors (experimental studies).

Reference	Solar concentrator	Electrical efficiency	Thermal capture efficiency	Maximum heat temperature	Research method
Liang et al. [59]	Non-concentrating	18.8 %	4.2 % at 45 °C	~45 °C	Experiment
Kandil et al. [45]	Fresnel lens	7–8 %	N/A	N/A	Experiment
Wingert et al. [21]	Parabolic trough	2.6–3.5 %	N/A	N/A	Experiment
This study	Fresnel lens	6.5 %	8.8 % at 80 °C	209.1 °C	Experiment

both high electrical efficiency and elevated operating temperatures [56], the available experimental results indicate that there is still considerable room for improvement in optical alignment, thermal management, and overall system integration to enhance electrical efficiency and achieve higher operating temperatures in future research.

4. Conclusion

This study demonstrates the feasibility and performance potential of spectral-splitting photovoltaic-thermal (PVT) collectors employing a dielectric Bragg mirror as a spectral-splitting optical filter for thermal-electrical decoupling. The results highlight not only the effectiveness of this spectral-splitting strategy but also the critical importance of detailed optical characterisation and angular analysis in the design of such reflectors, particularly under concentrated illumination.

By spectrally separating the solar spectrum, reflecting ultraviolet and visible wavelengths to a GaAs photovoltaic cell and transmitting low-energy, infrared photons to a thermal absorber, the system achieves a meaningful decoupling of electrical and thermal pathways. The Bragg mirror's angularly weighted cutoff wavelength of 870 nm closely matches the GaAs bandgap (870 nm), enabling effective spectral matching. Despite optical reflection losses of 8.6 % below the bandgap, the electrical efficiency is preserved at 6.5 % owing to a measured 5.2 K reduction in the PV cell encapsulation temperature. Although the absolute electrical performance remains lower than expected due to thermal and alignment-related losses under concentration, the system demonstrates high thermal performance, with a peak absorber block temperature of 209.1 °C and a thermal efficiency of 8.8 % at 80 °C.

The techno-economic performance strongly depends on specific climatic and operational conditions such as solar irradiance, ambient temperature, and system configuration. Nevertheless, all components used in the present prototype, including the Fresnel lens, GaAs photovoltaic cell, and solar thermal absorber, are commercially available. The only additional optical component compared with conventional concentrated photovoltaic or concentrated solar thermal systems is the Bragg mirror. Based on recent consultations with manufacturers, the current cost of small-area dielectric Bragg mirrors is on the order of 1000 to 10,000 USD/m^2. While this cost remains relatively high at present, the required Bragg-mirror area in a concentrated system can be significantly reduced by placing the mirror near the focal region of the solar concentrator through optimized optical design. Moreover, emerging scalable fabrication techniques, such as inkjet-printed dielectric multilayers, offer a promising pathway toward low-cost, large-area Bragg mirrors. With continued progress in this area, the proposed spectral-splitting hybrid system could become a feasible and competitive option for large-scale solar energy conversion.

Overall, the findings validate the spectral-splitting approach as a promising pathway toward hybrid solar energy systems that concurrently deliver heat and electricity. It should be noted that the primary aim of this study is to provide a comprehensive investigation of the spectral-splitting performance of Bragg mirrors for hybrid PVT collectors. Significant potential remains for improving both electrical and thermal efficiencies through optimized optical alignment, thermal management, and system integration. Based on the energy flow and distribution shown in Fig. 3d, both electrical and thermal efficiencies have the potential to exceed 20 % in future optimized designs. While the application of a Bragg mirror behind a Fresnel concentrator presents optical design challenges, these can be addressed through rigorous ray-tracing analysis and angular optimisation. The Bragg-mirror spectral-splitting concept, as demonstrated here, provides a scalable and tuneable architecture for next-generation PVT systems. In practical large-scale systems, dynamic adjustment of the Bragg mirror may be a solution to compensate for focal shifts and optical aberrations under outdoor operating conditions, ensuring consistent spectral-splitting and optical efficiency. Future improvements, including enhanced optical alignment, anti-reflective coatings, advanced thermal insulation, and refined Bragg mirror design, will be essential to fully unlock the potential of spectral-splitting PVT technologies in both low- and high-temperature applications.

CRediT authorship contribution statement

Botho Lehmann: Writing – review & editing, Writing – original draft, Methodology, Investigation, Formal analysis, Data curation, Conceptualization. **Gan Huang:** Writing – review & editing, Writing – original draft, Supervision, Methodology, Investigation, Funding acquisition, Formal analysis, Conceptualization.

Declaration of competing interest

The authors declare that they have no known competing financial interests or personal relationships that could have appeared to influence the work reported in this paper.

Acknowledgements

The authors gratefully acknowledge financial support received from: i) Helmholtz Investigator Group (G.H.). ii) the Helmholtz Association Research Field Energy: Program Materials and Technologies for the Energy Transition (Topic 1 Photovoltaics and Wind Energy, ref. 38.01.04); iii) the Karlsruhe School of Optics and Photonics (KSOP). The authors also wanted to thank Dr. Dmitry Busko for the support in calibrating the spectrum distribution of the solar simulator, and thank Prof. Bryce S. Richards for valuable discussion.

Appendix A. Supplementary data

Supplementary data to this article can be found online at https://doi.org/10.1016/j.solener.2025.114288.

Data availability

All data generated or analysed during this study are included in the published article and/or its Supplementary Information. Additional original and unprocessed data used in the article, as well as in the Supplementary Information, are available from the corresponding author upon reasonable request.

References

[1] Innovation Landscape for Smart Electrification: Power-to-Heat and Cooling - Status. International Renewable Energy Agency. https://www.irena.org/Innovation-landscape-for-smart-electrification/Power-to-heat-and-cooling/Status [Access date: 01 April 2025].
[2] Emissions Trends and Drivers. In: Climate Change 2022 - Mitigation of Climate Change: Working Group III Contribution to the Sixth Assessment Report of the

Intergovernmental Panel on Climate Change. Intergovernmental Panel on Climate Change, 2023; pp. 215-294.
[3] Abora, https://abora-solar.com/ [Access date: 12 August 2025].
[4] Fraunhofer ISE, PVTgen2 – Optimized PVT Collectors for Combined Electricity and Heat Generation. https://www.ise.fraunhofer.de/en/research-projects/pvtgen2.html [Access date: 30-10-2025].
[5] M.A. Green, E.D. Dunlop, M. Yoshita, N. Kopidakis, K. Bothe, G. Siefer, D. Hinken, M. Rauer, J. Hohl-Ebinger, X. Hao, Solar cell efficiency tables (Version 64), Prog. Photovolt. Res. Appl. 32 (7) (2024) 425–441.
[6] NREL, Champion Photovoltaic Module Efficiency Chart, https://www.nrel.gov/pv/module-efficiency [Access date: 30-10-2025].
[7] M. Herrando, A. Ramos, Photovoltaic-thermal (PV-T) systems for combined cooling, heating and power in buildings: a review, Energies 15 (9) (2022) 3021.
[8] A. Mellor, A.D. Alvarez, I. Guarracino, A. Ramos, R. Lacasta, F. Llin, A.J. Murrell, D.J. Paul, D. Chemisana, C.N. Markides, N.J. Ekins-Daukes, Roadmap for the next-generation of hybrid photovoltaic-thermal solar energy collectors, Sol. Energy 174 (2018) 386–398.
[9] G. Huang, et al., Challenges and opportunities for nanomaterials in spectral splitting for high-performance hybrid solar photovoltaic-thermal applications: A review, Nano Mater. Sci. 2 (3) (2020) 183–203.
[10] Technology Position Paper: PVT Collectors and System Concepts. IEA Solar Heating and Cooling Technology Collaboration Programme. https://www.iea-shc.org/Data/Sites/1/publications/IEA-SHC-Task60-PVT-Technology-Position-Paper.pdf [Access date: 01 April 2025].
[11] M.A. Green, et al., Solar cell efficiency tables (Version 64), Prog. Photovolt. Res. Appl. 32 (7) (2024) 425–441.
[12] C. Sun, et al., Temperature effect of photovoltaic cells: a review, Adv. Compos. Hybrid Mater. 5 (4) (2022) 2675–2699.
[13] X. Ju, C. Xu, X. Han, X. Du, G. Wei, Y. Yang, A review of the concentrated photovoltaic/thermal (CPVT) hybrid solar systems based on the spectral beam splitting technology, Appl. Energy 187 (2017) 534–563.
[14] G. Huang, S.R. Curt, K. Wang, C.N. Markides, Challenges and opportunities for nanomaterials in spectral splitting for high-performance hybrid solar photovoltaic-thermal applications: a review, Nano Mater. Sci. 2 (3) (2020) 183–203.
[15] A. Mojiri, R. Taylor, E. Thomsen, G. Rosengarten, Spectral beam splitting for efficient conversion of solar energy—A review, Renew. Sustain. Energy Rev. 28 (2013) 654–663.
[16] M. Herrando, K. Wang, G. Huang, T. Otanicar, O.B. Mousa, R.A. Agathokleous, et al., A review of solar hybrid photovoltaic-thermal (PV-T) collectors and systems, Prog. Energy Combust. Sci. 97 (2023) 101072.
[17] H. Liang, F. Wang, L. Yang, Z. Cheng, Y. Shuai, H. Tan, Progress in full spectrum solar energy utilisation by spectral beam splitting hybrid PV/T system, Renew. Sustain. Energy Rev. 141 (2021) 110785.
[18] R.A. Taylor, T. Otanicar, G. Rosengarten, Nanofluid-based optical filter optimisation for PV/T systems, Light Sci. Appl. 1 (10) (2012) e34–e.
[19] L. Huaxu, W. Fuqiang, C. Ziming, S. Yong, L. Bo, P. Yuzhai, Performance study on optical splitting film-based spectral splitting concentrated photovoltaic/thermal applications under concentrated solar irradiation, Sol. Energy 206 (2020) 84–91.
[20] T.P. Otanicar, S. Theisen, T. Norman, H. Tyagi, R.A. Taylor, Envisioning advanced solar electricity generation: Parametric studies of CPV/T systems with spectral filtering and high temperature PV, Appl. Energy 140 (2015) 224–233.
[21] R. Wingert, H. O'Hern, M. Orosz, P. Harikumar, K. Roberts, T. Otanicar, Spectral beam splitting retrofit for hybrid PV/T using existing parabolic trough power plants for enhanced power output, Sol. Energy 202 (2020) 1–9.
[22] L. Huaxu, W. Fuqiang, Z. Dong, C. Ziming, Z. Chuanxin, L. Bo, X. Huijin, Experimental investigation of cost-effective ZnO nanofluid based spectral splitting CPV/T system, Energy 194 (2020) 116913.
[23] L. Huaxu, W. Fuqiang, L. Dong, Z. Jie, T. Jianyu, Optical properties and transmittances of ZnO-containing nanofluids in spectral splitting photovoltaic/thermal systems, Int. J. Heat Mass Transf. 128 (2019) 668–678.
[24] S.S. Chougule, A. Srivastava, G.G. Bolegave, B.A. Gaikwad, P.M. Shirage, C. N. Markides, Next-generation solar technologies: Unlocking the potential of Ag-ZnO hybrid nanofluids for enhanced spectral-splitting photovoltaic-thermal systems, Renew. Energy 236 (2024) 121405.
[25] W. An, J. Zhang, T. Zhu, N. Gao, Investigation on a spectral splitting photovoltaic/thermal hybrid system based on polypyrrole nanofluid: preliminary test, Renew. Energy 86 (2016) 633–642.
[26] X. Xia, X. Cao, N. Li, B. Yu, H. Liu, Study on a spectral splitting photovoltaic/thermal system based on CNT/Ag mixed nanofluids, Energy 271 (2023) 127093.
[27] G. Zhang, S. Shan, H. Wu, J. Tian, Z. Cheng, Z. Zhou, Investigation on the radiative characteristics of ZnO-SiO_2 nanofluids in spectral splitting photovoltaic/thermal systems, Sol. Energy Mater. Sol. Cells 277 (2024) 113129.
[28] Y. Xiao, Y. Bao, L. Yu, X. Zheng, G. Qin, M. Chen, M. He, Ultra-stable carbon quantum dot nanofluids as excellent spectral beam splitters in PV/T applications, Energy 273 (2023) 127159.
[29] M.U. Sajid, Y. Bicer, Nanofluids as solar spectrum splitters: a critical review, Sol. Energy 207 (2020) 974–1001.
[30] G. Huang, K. Wang, S.R. Curt, B. Franchetti, I. Pesmazoglou, C.N. Markides, On the performance of concentrating fluid-based spectral-splitting hybrid PV-thermal (PV-T) solar collectors, Renew. Energy 174 (2021) 590–605.
[31] C. Zhang, C. Shen, Y. Zhang, C. Sun, D. Chwieduk, S.A. Kalogirou, Optimization of the electricity/heat production of a PV/T system based on spectral splitting with Ag nanofluid, Renew. Energy 180 (2021) 30–39.
[32] J. Xu, B. Chen, K. Yuan, J. Shu, Q. Yang, Optimization and performance assessment of Ag@ SiO_2 core–shell nanofluids for spectral splitting PV/T system: Theoretical and experiment analysis, Sol. Energy 283 (2024) 113030.
[33] Y. Ma, X. Han, Z. Chen, A.A. Khosa, Performance analysis of a nanofluid spectral splitting concentrating PV/T system with triangular receiver based on MCRT-FVM coupled method, Appl. Therm. Eng. 239 (2024) 122096.
[34] C. Xiong, X. Zhang, Q. Fu, M. Hu, M. Ma, S. Qing, H. Wang, Experimental investigation on the Magnetically controlled performance of Fe_3O_4@ SiO_2 nanofluids in a PV/T spectrum splitting system, Sol. Energy 287 (2025) 113244.
[35] J. Xu, B. Chen, J. Shu, K. Yuan, Q. Yang, A review of nanofluids-based spectral splitters: Characteristic, simulation, and experiment for PV/T hybrid system in utilization of full solar spectrum, Int. J. Green Energy (2025) 1–27.
[36] M. Pei, H. Liu, X. Ju, X. Ju, C. Xu, Investigation and optimization of the performance of a spectrum splitting photovoltaic/thermal system using multiple kinds of core-shell nanofluids, Energy 288 (2024) 129846.
[37] Y. Jiao, M. Xing, P. Estellé, Efficient utilization of hybrid photovoltaic/thermal solar systems by nanofluid-based spectral beam splitting: A review, Sol. Energy Mater. Sol. Cells 265 (2024) 112648.
[38] C. Shou, et al., Investigation of a broadband TiO_2/SiO_2 optical thin–film filter for hybrid solar power systems, Appl. Energy 92 (2012) 298–306.
[39] K. Lu, Q. Yu, B. Zhao, G. Pei, Performance analysis of a novel PV/T hybrid system based on spectral beam splitting, Renew. Energy 207 (2023) 398–406.
[40] T. Hu, T.H. Kwan, H. Yang, L. Wu, W. Liu, Q. Wang, G. Pei, Photothermal conversion potential of full-band solar spectrum based on beam splitting technology in concentrated solar thermal utilization, Energy 268 (2023) 126763.
[41] T. Jiang, T. Zou, G. Wang, J. Lin, Y. Duan, H. Peng, H. Chen, Design and thermodynamic analysis of an innovative parabolic trough photovoltaic/thermal system with film-based beam splitter, Case Stud. Therm. Eng. 47 (2023) 103093.
[42] Q. Zhang, Q. Jin, A. Mertens, C. Rainer, R. Huber, J. Fessler, et al., Fabrication of Bragg mirrors by multilayer inkjet printing, Adv. Mater. 34 (33) (2022) 2201348.
[43] Q. Jin, Q. Zhang, C. Rainer, H. Hu, J. Chen, T. Gehring, et al., Inkjet-printed optical interference filters, Nat. Commun. 15 (1) (2024) 3372.
[44] E. Yin, Q. Li, High-efficiency dynamic lossless coupling of a spectrum splitting photovoltaic-thermoelectric system, Energy 282 (2023) 128294.
[45] A.A. Kandil, E.M. Mokheimer, M.M. Awad, M.S. Salem, H.M. Bahaidarah, Maximizing exergy and energy efficiency in PV/TEG hybrid systems through beam splitting under best concentration conditions, Appl. Therm. Eng. (2025) 127324.
[46] H. Zhu, Z. Luo, Q. Cheng, L. Lu, Highly efficient spectrum-splitting solar energy utilization based on near-and far-field thermophotovoltaics, Energy 309 (2024) 133137.
[47] X. Chen, Y. Ji, G. Wu, J. Zang, L. Lu, Y. Zhang, H. Liang, Optical and thermal performance of a spectral-splitting transmission/photovoltaic system for plant factories, Energy 336 (2025) 138304.
[48] Y. Tian, P. Hadikhani, N. Alati, B.S. Richards, G. Huang, Hybrid solar spectral-splitting photovoltaic-thermal hydrogen production systems, Adv. Sci. (2025) 2503205.
[49] N.J. Liew, Z.J. Yu, Z. Holman, H.J. Lee, Application of spectral beam splitting using wavelength-selective filters for photovoltaic/concentrated solar power hybrid plants, appl. Therm. Eng. 201 (2022) 117823.
[50] Y. Ji, L.E. Artzt, W. Adams, C. Spitler, K. Islam, D. Codd, M.D. Escarra, A transmissive concentrator photovoltaic module with cells directly cooled by silicone oil for solar cogeneration systems, Appl. Energy 288 (2021) 116622.
[51] D.S. Codd, M.D. Escarra, B. Riggs, K. Islam, Y.V. Ji, J. Robertson, et al., Solar cogeneration of electricity with high-temperature process heat, Cell Rep. Phys. Sci. 1 (8) (2020).
[52] H. Liang, R. Su, W. Huang, Z. Cheng, F. Wang, G. Huang, D. Yang, A novel spectral beam splitting photovoltaic/thermal hybrid system based on semi-transparent solar cell with serrated groove structure for co-generation of electricity and high-grade thermal energy, Energ. Conver. Manage. 252 (2022) 115049.
[53] G. Huang, P.H. Arya, D.B. Ritzer, N.A. Alati, B. Abdollahi Nejand, U.W. Paetzold, B. S. Richards, Hybrid Perovskite-Photovoltaic and Solar-Thermal Harvesting, Adv. Sci. (2025) e09692.
[54] W. Skelton, Y. Ji, L. Artzt, C. Spitler, G. Ingrish, K. Islam, et al., Design and field testing of a sunflower hybrid concentrator photovoltaic-thermal receiver, Cell Rep. Phys. Sci. 3 (5) (2022).
[55] A.G. Imenes, D. Buie, D. McKenzie, The design of broadband, wide–angle interference filters for solar concentrating systems, Sol. Energy Mater. Sol. Cells 90 (11) (2006) 1579–1606.
[56] G. Huang, K. Wang, C.N. Markides, Efficiency limits of concentrating spectral-splitting hybrid photovoltaic-thermal (PV-T) solar collectors and systems, Light Sci. Appl. 10 (1) (2021) 28.
[57] C. Kittel, Introduction to Solid State Physics, Wiley, 1976.
[58] G. Huang, C.N. Markides, Spectral-splitting hybrid PV-thermal (PV-T) solar collectors employing semi-transparent solar cells as optical filters, Energ. Conver. Manage. 248 (2021) 114776.
[59] H. Liang, H. Han, F. Wang, Z. Cheng, B. Lin, Y. Pan, J. Tan, Experimental investigation on spectral splitting of photovoltaic/thermal hybrid system with two-axis sun tracking based on SiO2/TiO2 interference thin film, Energ. Conver. Manage. 188 (2019) 230–240.